Scientific Research Publishing

Open Journal of Civil Engineering, 2022, 12, 189-207
https://www.scirp.org/journal/ojce
ISSN Online: 2164-3172
ISSN Print: 2164-3164

Numerical Analysis of the Structure of High-Strength Double-Layer Steel Plate Concrete Shaft by Drilling Method of Water-Bearing Weak Rock Formation

Touogam Touolak Benedicte

School of Civil Engineering and Architecture, Anhui University of Science and Technology, Huainan, China
Email: 994310735@qq.com

How to cite this paper: Benedicte, T.T. (2022) Numerical Analysis of the Structure of High-Strength Double-Layer Steel Plate Concrete Shaft by Drilling Method of Water-Bearing Weak Rock Formation. *Open Journal of Civil Engineering*, **12**, 189-207.
https://doi.org/10.4236/ojce.2022.122012

Received: April 9, 2022
Accepted: May 24, 2022
Published: May 27, 2022

Abstract

In order to ensure the safety of coal mine shaft construction, a double-layer steel plate concrete composite shaft wall structure was proposed. However, fewer studies were conducted on this structure, which made engineers too confused to fully recognize its feasibility of this structure. Hence, based on the previous experimental research on the Taohutu mine construction project in Ordos in Inner Mongolia, this research paper aims to provide a widely deep numerical analysis by the usage of the finite element software, in fact, to establish the corresponding numerical analysis model and make a comparison with the experimental data to get the rationality of the verified model. The influence of the composite characteristics of the steel plate and concrete on the ultimate bearing capacity and stress field of the shaft wall structure is studied here through the method of multi-factor analysis. Also, the optimal design scheme of the double-layer steel plate and concrete composite shaft wall structure is proposed in this research paper.

Keywords

Finite Element Method, Double-Layer Steel Plate, Shaft Wall Structure, Taohutu Mine Construction

1. Introduction

China is the largest producer and consumer of coal in the world, and the development of coal resources, particularly in western China, is expected to continue at a constant pace for the present and future generations. According to the geological exploration data, in the western regions of Inner Mongolia, Shaanxi,

Gansu and other regions, deep water-bearing and weak rock formations are being formed at present and also when the new mine shafts will be built in the future. Most of them are Cretaceous and Jurassic rock formations with late diagenesis, weak cementation, low strength, and sanding and mudding in case of water. Because such type of formation is rich in water and is a pore-fissure aquifer, the efficiency of grouting and sealing water is poor, which makes it difficult to withstand the ordinary construction method. Therefore, the geological complexity of the western regions requires a special method for well sinking Talebi *et al.* [1] [2] [3]. Our study aims to solve this practical engineering problem often encountered in the field of coal mine shaft construction.

The drilling method involves a large shaft drilling rig to break the rock and soil, and then mud is used to protect the wall and discharge slag. Next, the wellbore is drilled to the required diameter and depth, and the prefabricated well wall is sunk and suspended in the mud. Finally, the well is filled with cement. This process is called the mechanized and automated well sinking method. Compared with the freezing method, it has the advantages of good construction safety, high degree of mechanization, reliable well wall quality, and no risk of flooding in the annular space of the freezing hole after the completion of the well. The commonly used shaft wall structures include plain concrete shaft walls, reinforced concrete composite shaft walls, and steel plate reinforced concrete composite shaft walls (Zhelnin *et al.* [4] [5]). Among them, the double-layer steel plate reinforced concrete shaft wall structure has high support strength and good stability, so it is widely used in the construction of coal mine shafts.

However, there are only a few studies on the double-layer steel plate concrete shaft wall structure [5] [6] [7] [8], and most of the existing reports mainly focus on the single-layer steel plate concrete composite shaft wall structure. For example, Yao Zhishu *et al.* [9] showed that embedding steel plates in the inner layer of the traditional reinforced concrete shaft wall structure could greatly improve the mechanical characteristics of the structure, and the bearing capacity of the shaft wall structure was also increased by 1.839-1.859%. Based on these experimental results, the optimal design theory of steel plate concrete shaft wall structure has been proposed [10]. To further improve the reliability and mechanical characteristics of the concrete shaft wall structure, Yao Zhishu *et al.* [11] prepared a concrete load shaft wall structure mixed with steel fibers. Furthermore, Yao Zhishu *et al.* [12] studied the mechanical characteristics of the double-layer steel plate shaft wall structure through similar model tests. The results showed that such a composite structure reduced the resistance of concrete. Notably, the compressive strength increased by a factor of 1.73 - 1.92.

To boost the engineering applications of the double-layer steel plate load shaft wall structure, its design and calculation method have been proposed based on the elastic-plastic combined cylinder method. However, an effective numerical model for the double-layer steel plate shaft wall structure has not been proposed yet. Therefore, an optimal numerical analysis and design model for this structure

is in urgent demand by the scientific and engineering community.

This study is based on the Taohutu mine construction project in Ordos City, Inner Mongolia, and a numerical model is established for the double-layer steel plate shaft wall according to the project overview. Further, the optimal design scheme of concrete shaft wall structure is proposed to guide the engineering applications.

2. Project Overview

Taohutu Mine is a large-scale mine that is being built by Chengda Mining Co., Ltd. in Erdos City, Inner Mongolia. The vertical shaft development method is adopted, and the mine is designed with four shafts: main shaft, auxiliary shaft, central air shaft, and northern air shaft. The Beifengwell is designed with an inner diameter of 6.5 m and a depth of 744 m. The wellbore passes through the Quaternary loose layers in the shallow part and the Cretaceous and Jurassic strata in the lower part. It is planned to use the drilling method for construction. According to the entire data obtained by wellbore inspection, the strata exposed by the wellbore from old to new are as follows: Jurassic Yan'an Formation, Zhiluo Formation, Anding Formation, Lower Cretaceous Luohe Formation, and Quaternary Aeolian Sand. Their average thicknesses are 204.32, 166.21, 55.82, 351.23, and 30.05 m, respectively. According to the occurrence characteristics of groundwater, it is divided into four water-bearing rock layers (groups) and one water-retaining rock layer (group): the pore water layer of Quaternary loose layer, the Cretaceous Zhidan Group sandstone pore and fissure aquifer, the Jurassic Zhiluo Formation sandstone pore and fissure aquifer, Jurassic Yan'an Formation sandstone pore and fissure aquifer, and Jurassic Anding Formation mudstone aquifer.

3. Numerical Analysis Model

3.1. Establishment of Numerical Model

Under the action of horizontally distributed load, the structure and load of the wellbore are axisymmetric; it can be regarded as a plane strain model and a quarter of the wellbore structure is used for modeling. In the calculation process, the lateral pressure is applied step by step, and the concrete rupture is the final failure. If the stress value of an element meets the strength criterion at a certain level of load, the element is considered to be completely destroyed: its residual stiffness and strength are ignored, and the stress released by the element is redistributed throughout the structure to reach a new equilibrium. If many elements fail, a singular structural stiffness matrix appears or the iteration of the unbalanced force can diverge. In this case, the structure is considered to be damaged and the calculation is terminated. The load at this time is the ultimate bearing capacity of the well wall.

The inner diameter of Taohutu's north wind shaft is 6.5 m, and according to the theoretical analysis of the shaft wall structure, the main factors affecting the

bearing capacity of the shaft wall are the shaft thickness, the strength grade of concrete, and the thickness of inner and outer steel plates. Consequently, three levels of each factor are considered in this study, which are shown in Table 1.

To ensure the universality of the geometric parameters of wellbore, the relative thickness of the wellbore is represented by the dimensionless parameter λ, which is the ratio of the thickness of the wellbore to the inner radius of the wellbore. For well wall thicknesses of 0.7, 0.8, and 0.9, the aspect ratios are 0.2153, 0.2461, and 0.2769, respectively. The simulations are conducted using the orthogonal statistical table l9 (38) of the first regression, and a total of 9 analysis cases are required (see Table 2 for more details).

An elastic-plastic constitutive model is adopted for the steel plate, where it is assumed that the steel plate and concrete meet the single condition assumption. The bilinear isotropic strengthening model (BISO) is adopted for the plastic stage of the material, and the steel plate is considered to meet the Mises yield condition. A multi-linear strengthening constitutive model is adopted for the high-strength concrete, which satisfies the concrete material strength criterion (Willam-Warnke five-parameter criterion) of the ANSYS software. During the calculation, the elastic modulus of the steel plate is uniformly taken as 2.1×10^5 MPa, while the Poisson's ratio is taken as 0.30. The plastic tangential modulus is

Table 1. Level value of each factor obtained by simulation.

Standard Level	Well Wall Thickness/m	Compressive Strength of Concrete/MPa	Thickness of Inner Steel Plate/mm	Thickness of Outer Steel Plate/mm
1	0.70	60	15	10
2	0.80	70	25	15
2	0.90	80	35	20

Table 2. Orthogonal design table for borehole simulation.

Model Number	Thickness-Diameter Ratio	Concrete Strength Grade	Thickness of Inner Steel Plate/mm	Thickness of Outer Steel Plate/mm
S-1	0.2153	C60	15	10
S-2	0.2153	C70	25	15
S-3	0.2153	C80	35	20
S-4	0.2461	C60	25	20
S-5	0.2461	C70	35	10
S-6	0.2461	C80	15	15
S-7	0.2769	C60	35	15
S-8	0.2769	C70	15	20
S-9	0.2769	C80	25	10

obtained according to the uniaxial tensile test curve in Figures 3-8. For the parameter a (see Table 3), the yield stress of concrete is ft = 0.8 fr. Since the Poisson's ratio of C60-C80 high-strength concrete is between 0.20 and 0.28, three values of 0.20, 0.22, and 0.25 are used in this study. These concrete strength values are explained in the theoretical analysis. The material parameters of steel plate and concrete are shown in Table 3 and Table 4, and the parameters of Willam-Warnke quasi-measurement are shown in Table 5. For the numerical calculation, the elastic modulus, Poisson's ratio, plastic tangential modulus, and the yield stress of steel plates and concrete are required to be the same as the geometric parameters in the test model.

3.2. Numerical Model

The PLANE182 element type is used for the plane model and the key option of plane strain (PLANE STRAIN) is enabled, and the elastic and plastic properties of the material are selected before the inputting the material parameters related to the steel plate and concrete. To establish the geometric model of the shaft wall, the geometric parameters of the shaft wall S-1 must be implemented in Cartesian coordinates. The material parameters of the inner/outer steel plates and concrete must be specified to form a plane quadrilateral mesh. The contact surface between the steel plate and the concrete is divided into surface-surface contact elements. The divided well wall model is shown in Figure 1.

Table 3. Material parameters of steel plate (Unit: MPa).

Model Number	Elastic Modulus	Plastic Tangential Modulus	Poisson's Ratio	Yield Stress
S-1 to S-9	2.1 × 105	0.57 × 105	0.30	340

Table 4. Material parameters of high-strength concrete (Unit: MPa).

Model Number	Elastic Modulus/ ($\times 10^4$) MPa	Poisson's Ratio	Yield Stress/MPa	Plastic Tangential Modulus/ ($\times 10^4$) MPa	Cube Compressive Strength/MPa
S-1	3.87	0.20	48	3.66	60
S-2	4.07	0.22	56	3.66	70
S-3	4.25	0.25	64	3.66	80
S-4	3.87	0.20	48	3.66	60
S-5	4.07	0.22	56	3.09	70
S-6	4.25	0.25	64	3.27	80
S-7	3.87	0.20	48	3.41	60
S-8	4.07	0.22	56	3.52	70
S-9	4.25	0.25	64	3.61	80

Table 5. Willam-Warnke failure criterion for concrete.

Label	Parameter	Implication	Range of Values
1	ShrCf-Op	Shear transfer coefficient for open cracks	0 - 1
2	ShrCf-C1	Shear transfer coefficient for closed cracks	0 - 1
3	UnTensSt	Uniaxial tensile strength	$f_t = 0.395F_c^{0.55}$
4	UnCompSt	Uniaxial compressive strength	Obtained from the experimental results
5	Bierce	Biaxial compressive strength	$1.2F_c$
6	Hindus	Surrounding rock pressure	0.01 H
7	Bierce	Biaxial compressive strength under surrounding rock	$1.725F_c$
8	UnTensST	Uniaxial compressive strength under surrounding rock	$1.45F_c$

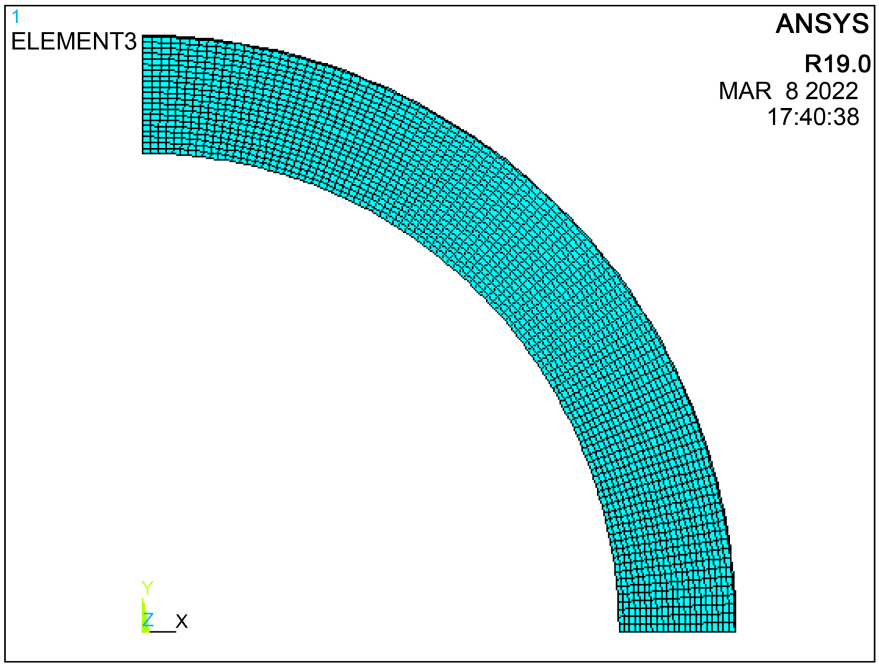

Figure 1. Numerical representation of the plane calculation model.

The plane calculation model includes applying a uniform radial line load to the outer wall in the solver of the model. There are two solution methods. The first one is to apply a larger external load, set appropriate time steps and sub-steps, and then apply an equal load to each step, and finally the solution of each sub-step is written into the result file. By following these steps, it is easy to obtain the stress results corresponding to each level of the load below the maximum load during the post-processing. It may be noted the corresponding strain

results cannot be obtained at this stage due to the large displacements that are embedded or deviation from the concrete surface to the inner and outer steel plates.

An alternative way is to go back to the solver and apply another level of load and then set the next loading step until the plate stress strength (Von Mises) exceeds the failure limit or the stress at a point in the concrete. The state falls outside the failure surface of the Willam-Warnke failure criterion in the stress space.

This method is fast and provides reliable results irrespective of the deformation. Therefore, in this study, the second method is used to find a certain horizontal load, while the first method is used to find the ultimate load. After implementing the post-processor, an overview of the main calculation results can be obtained. Furthermore, we can define a path along the radial direction and then input the position coordinates of some points to get the tangential direction, radial stress and strain, and the stress intensity of the points along the path.

4. Results and Discussion

4.1. Analysis of Stress Distribution Characteristics

To obtain the stress distribution characteristics, it is important to apply a confining pressure of 30 MPa to the model, then set the time sub-step to 30 so that each sub-step represents a load increment of 1 MPa, and finally obtain the inner and outer steel plates of each model from the post-processor POST26 before the limit bearing capacity is reached. Figures 2-10 show the variations in the radial stress and hoop stress as a function of the load before the concrete reaches the ultimate bearing capacity.

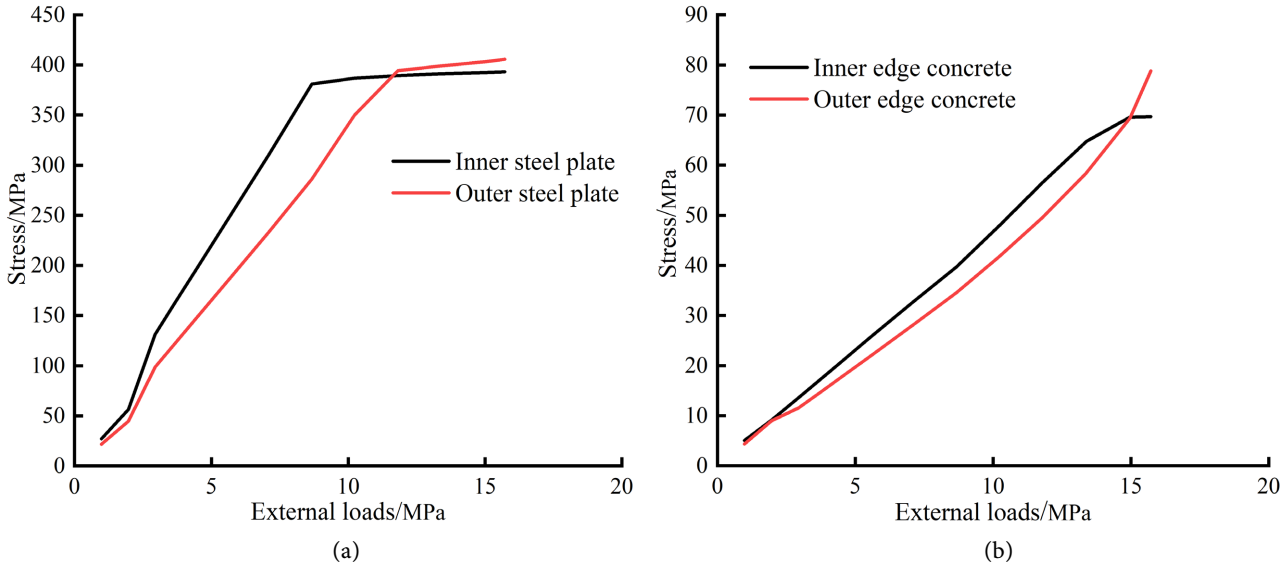

Figure 2. Hoop stress-confining pressure relationship curve of S-1 model. (a) Hoop stress vs. confining pressure curve of steel plate; (b) Hoop stress vs. confining pressure of concrete.

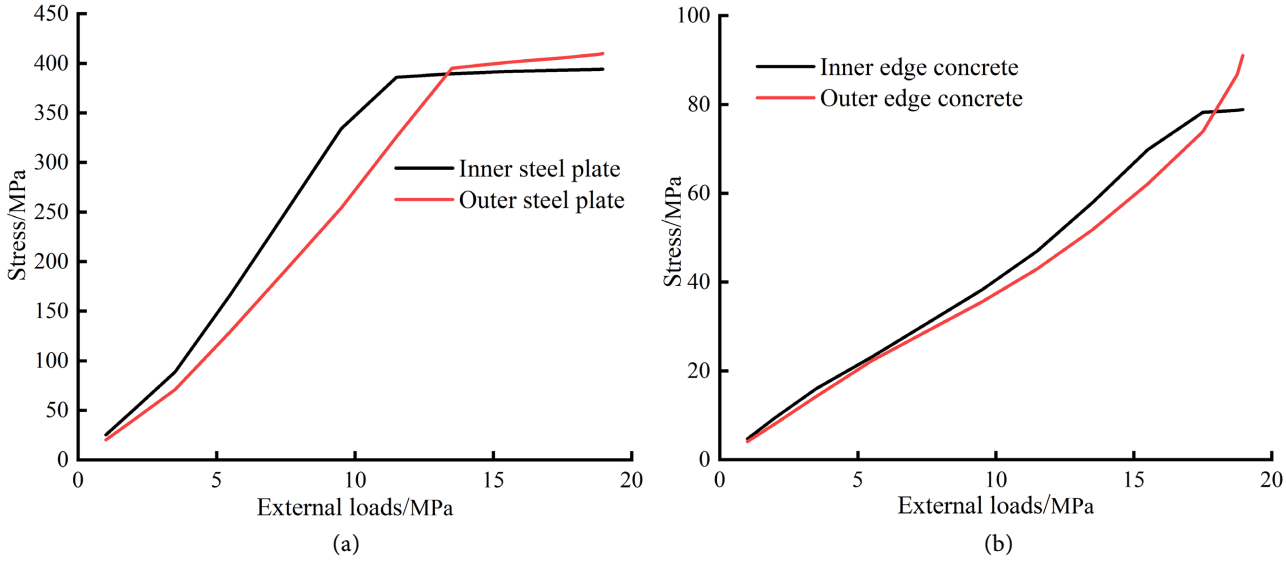

Figure 3. Hoop stress-confining pressure relationship curve of S-2 model. (a) Hoop stress vs. confining pressure curve of steel plate (b) Hoop stress vs. confining pressure of concrete.

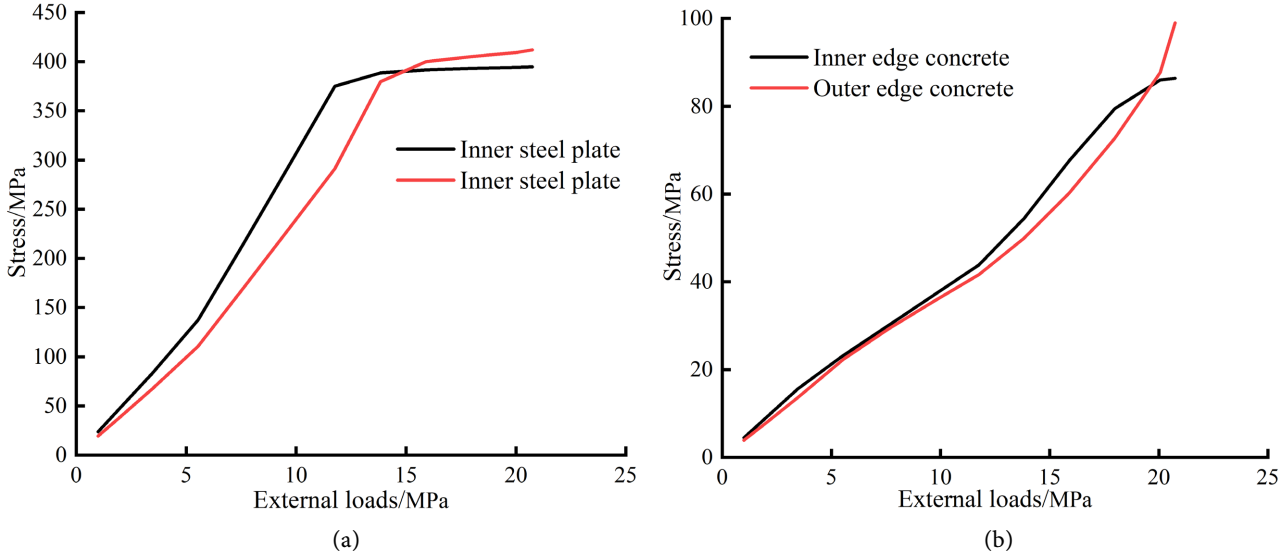

Figure 4. Hoop stress-confining pressure relationship curve of s-3 model. (a) Hoop stress vs. confining pressure curve of steel plate; (b) Hoop stress vs. confining pressure of concrete.

It can be seen in Figures 2-10 that when the external load is applied to the shaft wall, the hoop stress growth rate of the inner steel plate is larger that of the outer steel plate. Therefore, when the hoop stress of the inner steel plate layer reaches the maximum value, the hoop stress of the outer steel plate layer continues to increase beyond that of the inner layer and reaches the maximum value later. When the external load (less than 10 MPa) is applied to the shaft wall, the variation trends as well as the growth rates of the hoop stress of concrete at the inner and outer edges are the same. Notably, the hoop stress growth rate of the concrete on the inner edge is slightly larger than that on the outer edge when the

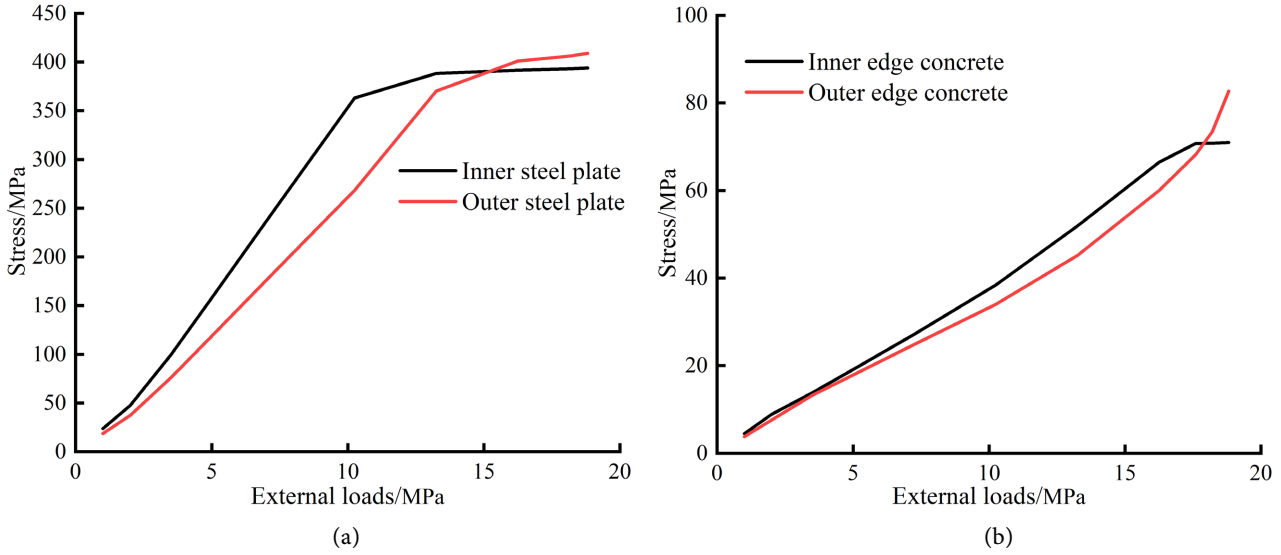

Figure 5. Hoop stress-confining pressure relationship curve of s-4 model. (a) Hoop stress vs. confining pressure curve of steel plate; (b) Hoop stress vs. confining pressure of concrete.

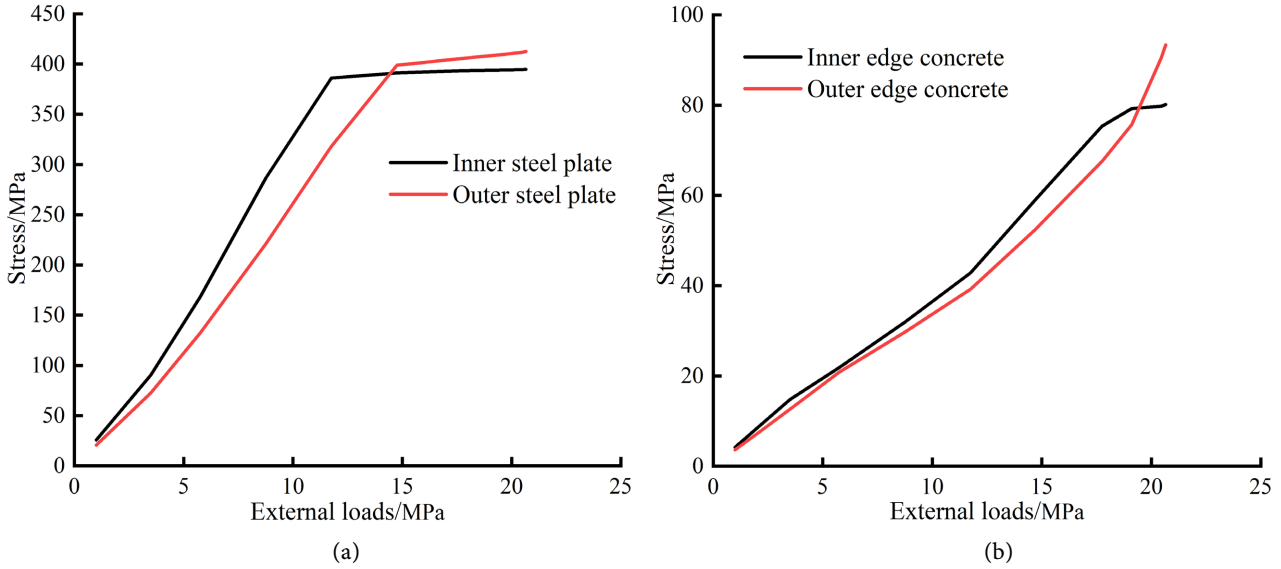

Figure 6. Hoop stress-confining pressure relationship curve of S-5 model. (a) Hoop stress vs. confining pressure curve of steel plate; (b) Hoop stress vs. confining pressure of concrete.

external load is greater than 10 MPa. Further, the hoop stress gradually reaches the maximum value under the ultimate load stress.

The above simulation results suggest that the concrete on the outer edge of the shaft wall may reach its yield strength first, and then its fails under the ultimate load of the steel plate-concrete composite shaft wall. The simulated relationship between the hoop stress and the confining pressure of the inner and outer steel plates is approximately consistent with that obtained by the test, which verifies the feasibility of the proposed model. The relationship between the hoop stress of concrete on the inner and outer edge and the confining pressure is also

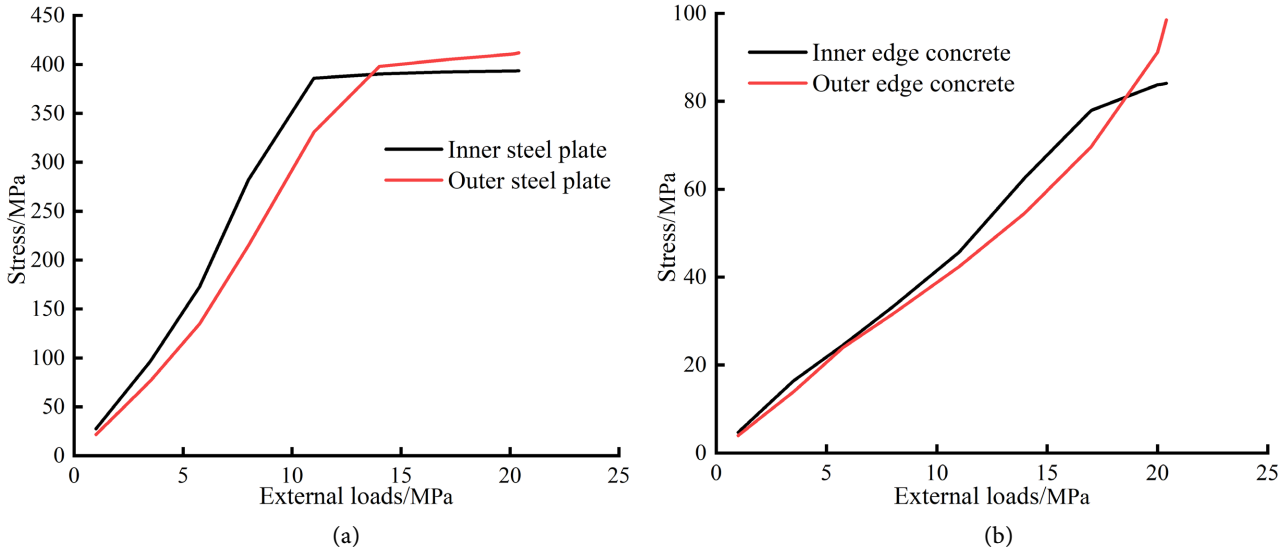

Figure 7. Hoop stress-confining pressure relationship curve of S-6 model. (a) Hoop stress vs. confining pressure curve of steel plate; (b) Hoop stress vs. confining pressure of concrete.

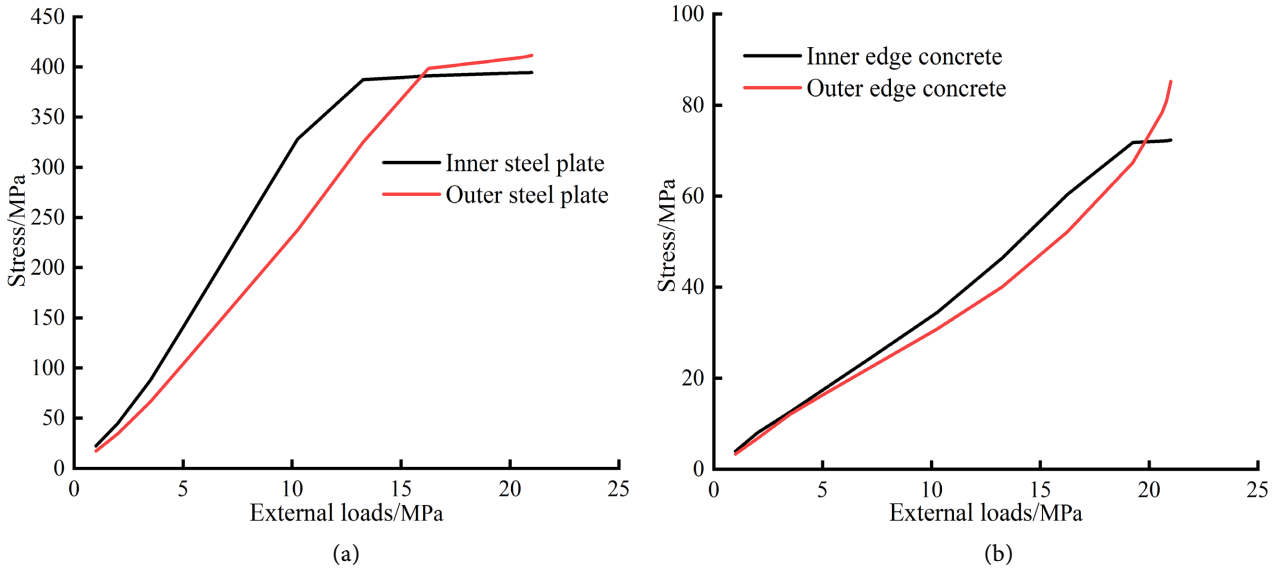

Figure 8. Hoop stress-confining pressure relationship curve of S-7 model. (a) Hoop stress vs. confining pressure curve of steel plate; (b) Hoop stress vs. confining pressure of concrete.

similar to that obtained by the test. Thus, it is inferred that the numerical calculation with ANSYS program fully reflects the variation law of hoop stress of concrete with confining pressure.

Therefore, the ANSYS software is effective for examining the borehole wall. Besides, the bearing capacity of the shaft wall and its main influencing factors are analyzed by ANSYS numerical calculation.

4.2. Analysis of Borehole Wall Bearing Capacity

The finite element software ANSYS is used for the numerical analysis of many

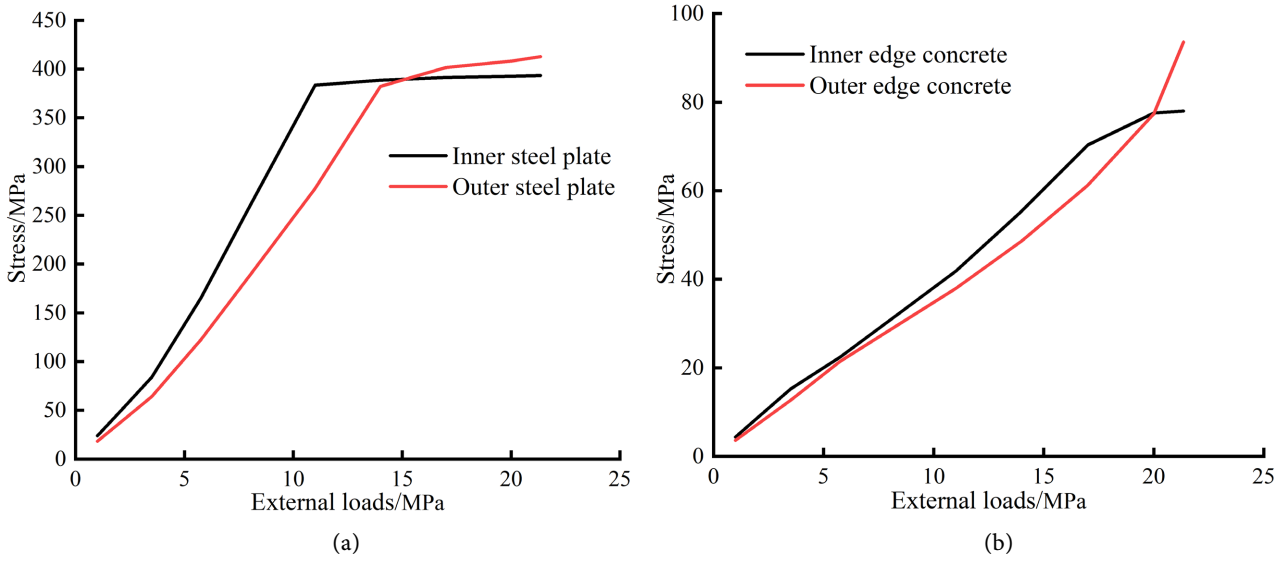

Figure 9. Hoop stress-confining pressure relationship curve of S-8 model. (a) Hoop stress vs. confining pressure curve of steel plate; (b) Hoop stress vs. confining pressure of concrete.

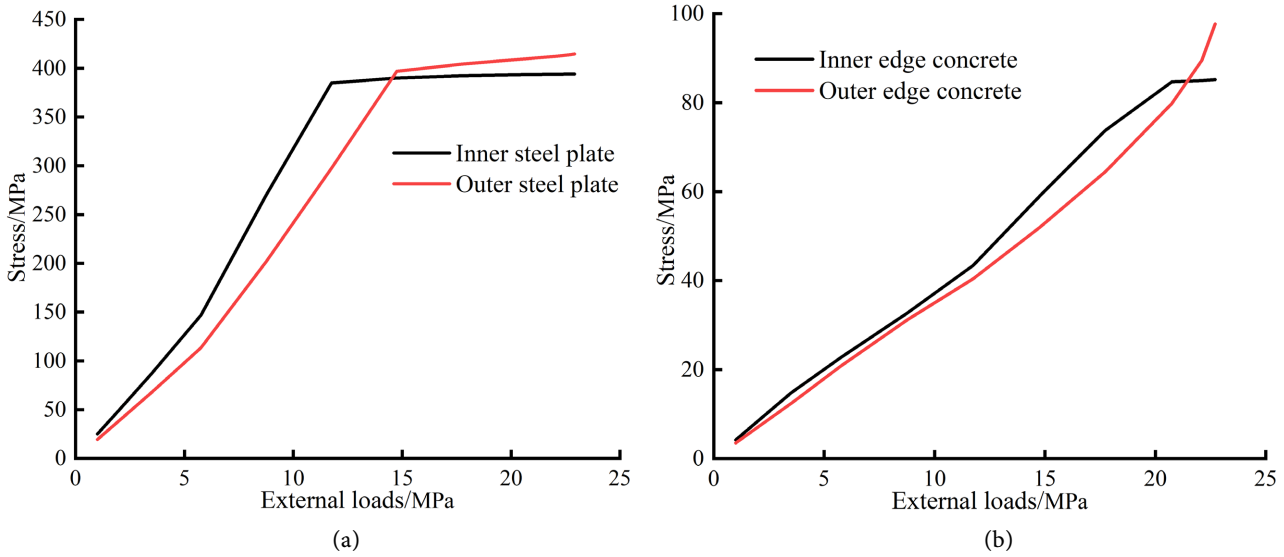

Figure 10. Hoop stress-confining pressure relationship curve of S-9 model. (a) Hoop stress vs. confining pressure curve of steel plate; (b) Hoop stress vs. confining pressure of concrete.

engineering structures, and it can provide many parameters such as stress and strain under any load level. However, due to the fine element division and numerical simulation errors, the ANSYS program cannot identify when the wellbore begins to fail. Further, there are many false eigenvalues, which makes it difficult to assess the correct limit value, even if the characteristic value of critical load is obtained by buckling analysis.

Therefore, the element table in the post-processor is used to substitute the stress results solved under each load level into the Willam-Warnke strength criterion, and then mathematical operations are performed on each node. When

the stress condition under a certain load level is satisfied, the Willam-Warnke criterion is used and the concrete is considered to have failed. According to the measured strains on the inner and outer surfaces of the shaft wall and the failure form in the test, it can be seen that when the concrete starts to fail, the concrete on the inner edge of the shaft wall firstly cracks before peeling off locally. After the cracking of the inner edge, the shaft wall model can continue to bear the load.

As the load increases, the failure surface expands from the inside to the outside. When the concrete on the outer edge also breaks, the shaft wall completely loses its bearing capacity. Therefore, when the Willam-Warnke concrete strength criterion is used, the concrete on the outer edge should reach the limit state of shaft wall failure. The ultimate bearing capacity of the nine wellbore models determined by numerical simulation is shown in Table 6.

The concrete strength criterion is strictly related to the bearing capacity during simulation. The Willam-Warnke strength criterion used in this study is also employed in the ordinary concrete structures; this result of this method is in good agreement with the test bearing capacity of the shaft wall structure.

Previous studies have shown that the bearing capacity obtained by ANSYS software is smaller than the experimental value obtained by a similar model test [1]. This can be attributed to the following reasons. Firstly, the high-strength concrete is in a composite shaft wall and its strength is improved due to the tightening effect of the double-layer steel plate. Another reason is the value of concrete parameters. The use of other criteria such as the Ottosen strength criterion to calculate the bearing capacity of the borehole wall was also explored in this study. Unfortunately, the obtained results were inferior to those obtained by the Willam-Warnke strength criterion. Therefore, the Willam-Warnke strength criterion can be used as a reference criterion for judging the failure of high-strength concrete in the shaft wall structure, if and only if the parameters can be corrected accordingly. It is important to note that the bearing capacity obtained by ANSYS software still reflects the strength characteristics of the shaft wall structure. However, the bearing capacity obtained by numerical calculation is more suitable than that obtained by experimental tests. In general, when the bearing capacity of the wall structure is smaller, a lot of waste material exists. This point is discussed in the next subsection. Moreover, since there is no restriction on the size of the model, the geometric parameters of the prototype can be selected for calculation, and then the calculated bearing capacity value will be

Table 6. Ultimate bearing capacity of shaft wall (MPa) obtained by numerical calculation.

Model	S-1	S-2	S-3	S-4	S-5	S-6	S-7	S-8	S-9
Concrete Strength	60	70	80	60	70	80	60	70	80
Bearing Capacity	15.72	18.95	21.76	18.82	20.65	20.41	21.01	21.35	22.91

relatively more accurate. Therefore, the qualitative and quantitative relationship between the ultimate bearing capacity of the shaft wall and the influencing factors such as aspect ratio, concrete strength, and inner/outer steel plates can be analyzed.

4.3. Influencing Factors of Borehole Wall Bearing Capacity

The main influencing factors of the ultimate bearing capacity of the steel plate concrete composite shaft wall are the thickness of the shaft wall concrete layer (which can be converted into the thickness-to-diameter ratio), concrete strength, and thicknesses of the inner and outer steel plates. For the Model S-1, the ANSYS program is used to calculate the bearing capacity of the shaft wall for a total of seven concrete grades from C50 to C80. The calculation results are shown in Table 7, and the relationship between the bearing capacity of the shaft wall and the concrete strength is shown in Figure 11.

Table 7. Calculated values of shaft wall bearing capacity under different concrete strength grades.

Concrete Strength Grade	C50	C55	C60	C65	C70	C75	C80
Elastic Modulus/MPa	36,400	37,600	38,700	39,700	40,700	41,600	42,500
Concrete Yield Stress/MPa	40	44	48	52	56	60	64
Concrete Plastic Tangential Modulus/MPa	30,900	32,700	34,100	35,200	36,600	37,800	38,700
Ultimate Bearing Capacity/MPa	13.9	14.6	15.7	16.5	17.7	18.9	20.2

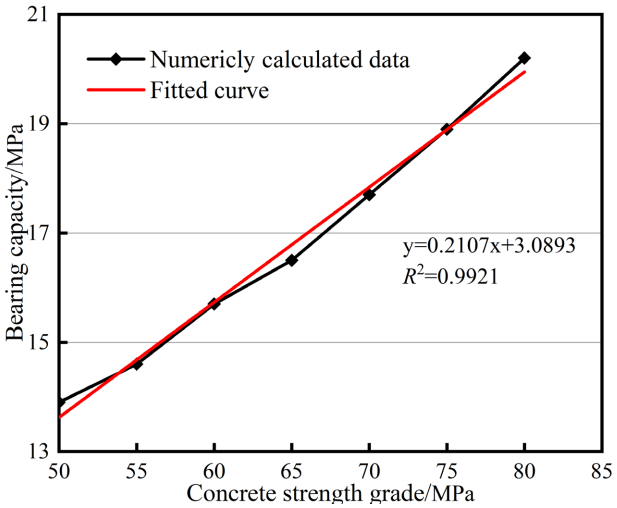

Figure 11. Variation in the shaft wall bearing capacity with the concrete strength grade.

It can be seen from Table 7 and Figure 11 that the concrete strength grade has a substantial effect on the bearing capacity of the shaft wall. Specifically, the bearing capacity of the shaft wall is approximately linearly proportional to the concrete strength. If the concrete strength grade is increased from C50 to C80, the ultimate bearing capacity of the shaft wall is increased by 8.3 MPa.

Further, the thickness of the concrete layer in the shaft wall has a significant impact on the bearing capacity of the concrete composite shaft wall. For Model S-1, the ANSYS calculation program is used to determine the borehole wall bearing capacity for thickness-diameter ratios from 0.2153 to 0.2769. The calculation results are shown in Table 8, and the relationship between the shaft wall bearing capacity and the thickness-diameter ratio is shown in Figure 12.

It is clear from Figure 12 that the bearing capacity of the well wall is also linearly proportional to the thickness-diameter ratio. When the thickness-diameter ratio increases from 0.2153 to 0.2769, the ultimate bearing capacity of the cell wall increases from 15.7 MPa to 19.2 MPa. However, the aspect ratio is not arbitrarily increased, which is related to the diameter of the drill bit and the cost of well construction.

Similarly, the thickness of the inner and outer steel plates can also affect the ultimate bearing capacity of the shaft wall. In general, the thickness of the inner steel plate is greater than or equal to that of the outer steel plate. To examine the influence of the inner steel plate thickness on the ultimate bearing capacity of the shaft wall, the thickness of the inner steel plate of the Model S-3 is gradually

Table 8. Calculated values of borehole wall bearing capacity under different thickness-diameter ratios.

Aspect Ratio	0.2153	0.2461	0.2769
Shaft Wall Bearing Capacity/MPa	15.7	17.5	19.2

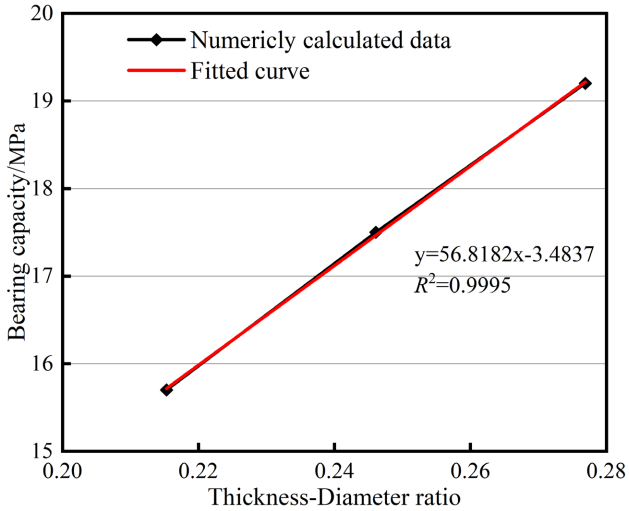

Figure 12. Well wall bearing capacity-thickness-diameter ratio relationship curve.

reduced from 35 mm to 15 mm with a step size of 5 mm. The ultimate bearing capacity of the shaft wall is shown in Table 9. Similarly, to reveal the influence of the outer steel plate thickness on the bearing capacity of the shaft wall, the thickness of the outer steel plate of the Model S-3 is increased from 15 mm to 35 mm in steps of 5 mm. The variation in the ultimate bearing capacity of the shaft wall as a function of the outer steel plate thickness, which is obtained by the ANSYS software, is shown in Table 10. The variation in the bearing capacity as a function of the thickness of the steel plates is presented in Figure 13 and Figure 14.

It can be seen in Figure 13 and Figure 14 that the ultimate bearing capacity varies linearly with the thickness of the steel plate. However, the bearing capacity does not increase significantly with the increase in the thickness of the steel plates. As shown in Table 11, when the inner steel plate thickness is increased from 15 mm to 35 mm, the bearing capacity is only increased by 2.31 MPa; when the outer steel plate thickness is increased from 15 mm to 35 mm, the bearing capacity is only increased by 1.97 MPa. Furthermore, increasing the thickness of

Table 9. Calculated values of shaft wall bearing capacity under different thicknesses of inner steel plate.

Inner Steel Plate Thickness/mm	15	20	25	30	35
Bearing Capacity/MPa	19.45	20.21	20.65	21.35	21.76

Table 10. Calculated values of shaft wall bearing capacity under different thicknesses of outer steel plate.

Outer Steel Plate Thickness/mm	15	20	25	30	35
Bearing Capacity/MPa	21.36	21.76	22.31	22.72	23.33

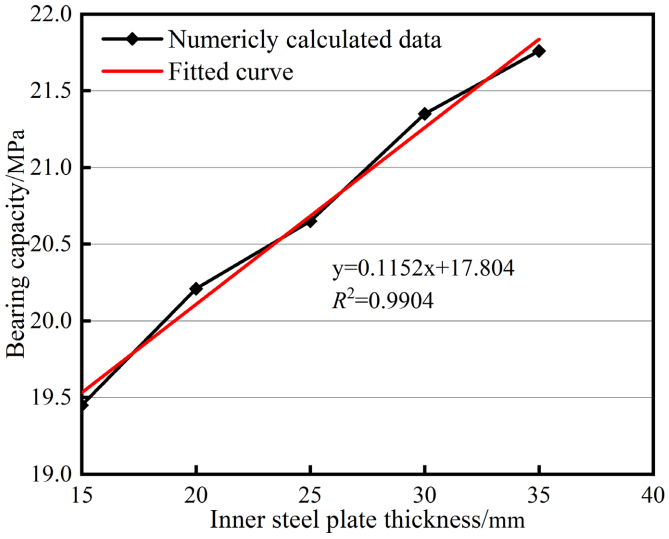

Figure 13. Relationship between the ultimate bearing capacity and inner steel plate thickness.

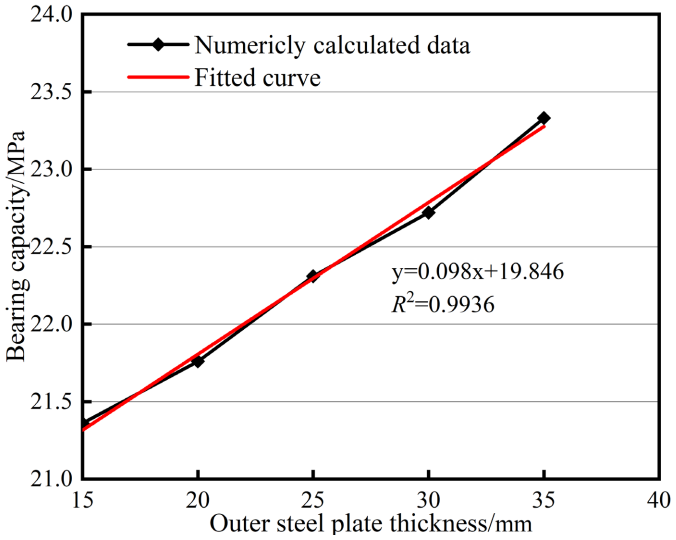

Figure 14. Relationship between the ultimate bearing capacity and thickness of outer steel plate.

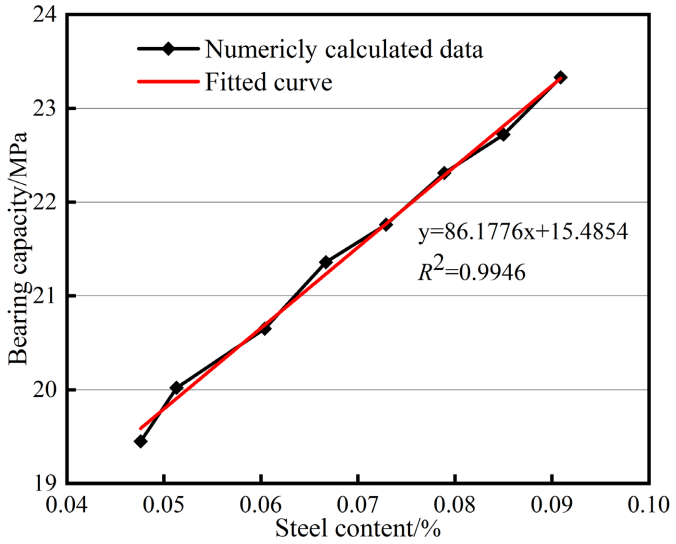

Figure 15. Variation in the shaft wall bearing capacity with the steel content of shaft wall section.

Table 11. Calculated values of shaft wall bearing capacity under different steel contents of shaft wall sections.

Steel Content of Shaft Wall Section	0.0476	0.0513	0.0604	0.0667	0.0729	0.0789	0.085	0.0909
Bearing Capacity/MPa	19.45	20.21	20.65	21.36	21.76	22.31	22.72	23.33

the inner steel plate is more efficient than increasing the thickness of the outer steel plate. This is mainly due to the action of lateral pressure, where the hoop stress in the section of the well wall is large on the inside and small on the out-

side. In this case, we can observe that the weak point belong to the inner side, while the strength is in the cell wall structure. By considering the processing limitations of the steel plate, the thickness of the inner and outer steel plates cannot be increased arbitrarily.

Now, we consider the effect of the steel content of the shaft wall section, where H1 and H2 are the thicknesses of the inner and outer steel plates, and δ is the thickness of the shaft wall. According to the above formula, the bearing capacity of shaft wall sections with different steel contents can be obtained when the thickness of the inner and outer steel plates changes.

It can be seen in **Figure 15** that since the thicknesses of the inner and outer steel plates have a minor effect on the bearing capacity of the shaft wall, regardless of the change in these thicknesses, the bearing capacity of the shaft wall is generally linearly proportional to the steel content. Therefore, the influence of the inner and outer steel plate thickness on the bearing capacity of the shaft wall can be analyzed through the steel content instead. According to the above analysis, it can be seen that the concrete strength and thickness-diameter ratio have the greatest influence on the bearing capacity of the shaft wall. However, considering the cost efficiency and the actual well construction situation, increasing the strength level of the concrete is the most effective method to improve the bearing capacity of the shaft wall.

5. Conclusions

Based on the Taohutu mine construction project in Ordos City, Inner Mongolia, a numerical model was established for the double-layer steel plate shaft wall according to the general situation of the project. Further, the composite characteristics of the steel plate and concrete structure were comprehensively examined, and a double-layer steel plate concrete shaft wall structure was proposed. The optimized design scheme, as well as the main results of this study, is summarized as follows:

1) The relationship between the hoop stress and confining pressure of the inner and outer steel plates was approximately consistent with that obtained by the test, which verified the rationality of the proposed numerical model. The numerical model reflected the variation laws of the hoop stress with the confining pressure at the inner and outer steel plates in the steel plate-concrete composite shaft wall.

2) The ultimate bearing capacity of the double-layer steel plate concrete composite shaft wall structure was linearly proportional to the thickness of the steel plate. However, despite the increase in the thickness of the steel plate, the bearing capacity did not increase significantly. When the thickness of the inner steel plate was increased from 15 mm to 35 mm, the bearing capacity only increased by 2.31 MPa; when the thickness of outer steel plate increased from 15 mm to 35 mm, the bearing capacity only increased by 1.97 MPa. Furthermore, increasing the thickness of the inner steel plate was found to be more efficient than in-

creasing the thickness of the outer steel plate.

3) The concrete strength and the diameter thickness-diameter ratio had the strongest impact on the bearing capacity of the double-layer steel plate concrete composite shaft wall structure. Considering the cost factor and the actual well construction situation, increasing the strength level of the concrete is the most effective method to improve the nearing capacity of the shaft wall structure.

Conflicts of Interest

The author declares no conflicts of interest regarding the publication of this paper.

References

[1] Talebi, S. and Young, R.P. (2021) Microseismic Monitoring in Highly Stressed Granite: Relation between Shaft-Wall Cracking and *in Situ* Stress. *International Journal of Rock Mechanics and Mining Sciences & Geomechanics Abstracts*, **29**, 25-34. https://doi.org/10.1016/0148-9062(92)91042-4

[2] Bavi, R., Hajnayeb, A., Sedighi, H.M. and Shishesaz, M. (2022) Simultaneous Resonance and Stability Analysis of Unbalanced Asymmetric Thin-Walled Composite Shafts. *International Journal of Mechanical Sciences*, **217**, 107047. https://doi.org/10.1016/j.ijmecsci.2021.107047

[3] Wang, Y.S., Zhang, C., Xue, L.B. and Huang, X.G. (2010) Prediction and Safety Analysis of Additional Vertical Stress within a Shaft Wall in an Extra-Thick Alluvium. *Mining Science and Technology*, **20**, 350-356. https://doi.org/10.1016/S1674-5264(09)60207-6

[4] Zhelnin, M., Kostina, A., Esina, E. and Plekhov, O. (2021) Calculation of the Stress-Strain State in a Shaft Lining during Thawing of the Frozen Wall. *Procedia Structural Integrity*, **32**, 71-78. https://doi.org/10.1016/j.prostr.2021.09.011

[5] Sungsoo, N., Hyungwon, Y. and Librescu, L. (2006) Effect of Taper Ratio on Vibration and Stability of a Composite Thin-Walled Spinning Shaft. *Thin-Walled Structures*, **44**, 362-371. https://doi.org/10.1016/j.tws.2006.02.007

[6] Xie, L.D., Gao, X.Y., Yang, Y., Zhi, Y.H. and Dong, Z.X. (2021) Optimization for Connected Steel Plates of Single-Layer Shaft Wall under Blasting Excavation by Numerical Simulation Method. *IOP Conference Series: Earth and Environmental Science*, **719**, Article No. 032013. https://doi.org/10.1088/1755-1315/719/3/032013

[7] Yao, Z.S., Zhang, P., Cheng, H., Xue, W.P. and Li, X. (2020) Testing of a Dual-Steel-Plate-Confined High-Performance Concrete Composite Shaft Lining Structure and Its Application. *Applied Sciences*, **10**, 2938. https://doi.org/10.3390/app10082938

[8] Cui, G.X. (1989) The Simulation Tests Principle of Freezing Method Sinking. *Journal of China University of Mining and Technology*, No. 1, 62-71.

[9] Yao, Z.S., Xue, W.P., Cheng, H., *et al.* (2018) Research on the Application of High-Strength Reinforced Concrete Composite Shaft Wall with Inner Steel Plate in Freezing Shaft. *Chinese Journal of Mining and Safety Engineering*, **35**, 663-669.

[10] Yao, Z.S., Cheng, H. and Rong, C.X. (2008) Experimental Study of High-Strength Reinforced Concrete Composite Shaft Wall of Deep-Frozen Shaft Inner Layer. *Chinese Journal of Rock Mechanics and Engineering*, No. 1, 153-160.

[11] Yao, Z.S., Cheng, H. and Ju, X.B. (2017) Research and Application of Inner Steel

Plate High-Strength Steel Fiber Reinforced Concrete Composite Wellborn Repairing Deep Alluvial Well-Born. *Chinese Journal of Coal*, **42**, 2295-2301.

[12] Yao, Z.S., Yu, G.H., Cheng, H., *et al*. (2010) Experimental Study on Vertical Bearing Capacity of Steel Plate Concrete Composite Shaft Wall with Extra-Thick Topsoil Layer. *Geotechnical Mechanics*, **31**, 1687-1691.